Published in final edited form as:
Cancer Discov. 2014 January ; 4(1): 80–93. doi:10.1158/2159-8290.CD-13-0642.

Acquired resistance and clonal evolution in melanoma during BRAF inhibitor therapy

Hubing Shi[#1,6], **Willy Hugo**[#1,6], **Xiangju Kong**[1,6], **Aayoung Hong**[1,5,6], **Richard C. Koya**[2,6], **Gatien Moriceau**[1,6], **Thinle Chodon**[3,6], **Rongqing Guo**[3,6], **Douglas B. Johnson**[7,10], **Kimberly B. Dahlman**[8,10], **Mark C. Kelley**[9,10], **Richard F. Kefford**[11], **Bartosz Chmielowski**[3,4,6], **John A. Glaspy**[3,4,6], **Jeffrey A. Sosman**[7,10], **Nicolas van Baren**[12], **Georgina V. Long**[11], **Antoni Ribas**[1,3,4,5,6], and **Roger S. Lo**[1,4,5,6]

[1]Division of Dermatology, Department of Medicine

[2]Division of Surgical Oncology, Department of Surgery

[3]Division of Hematology & Oncology, Department of Medicine

[4]Jonsson Comprehensive Cancer Center

[5]Department of Molecular and Medical Pharmacology

[6]David Geffen School of Medicine, University of California, LA, California 90095-1662 USA

[7]Department of Medicine

[8]Department of Cancer Biology

[9]Department of Surgery

[10]Vanderbilt-Ingram Cancer Center, Nashville, TN 37232

[11]Melanoma Institute of Australia, Westmead Millenium Institute, Westmead Hospital, University of Sydney, New South Wales, Australia

[12]Ludwig Institute for Cancer Research, Brussels Branch, Belgium

[#] These authors contributed equally to this work.

Abstract

BRAF inhibitors elicit rapid anti-tumor responses in the majority of patients with ^{V600}*BRAF* mutant melanoma, but acquired drug resistance is almost universal. We sought to identify the core resistance pathways and the extent of tumor heterogeneity during disease progression. We show that MAPK reactivation mechanisms were detected among 70% of disease-progressive tissues, with *RAS* mutations, mutant *BRAF* amplification and alternative splicing being most common. We also detected PI3K-PTEN-AKT-upregulating genetic alterations among 22% of progressive

Address for correspondence: Dr. Roger S. Lo at 52-121 CHS Dept. of Medicine/Dermatology, 10833 Le Conte Ave, Los Angeles, CA 90095-1750 or at rlo@mednet.ucla.edu..

Supplementary data for this article are available at Cancer Discovery Online (http://www.cancerdiscovery.aacrjournals.org).

Disclosure of Potential Conflicts of Interest: The authors (A.R. and R.S.L.) declare patent PCT Application Serial No. 13/879,302 (COMPOSITIONS AND METHODS FOR DETECTION AND TREATMENT OF B-RAF INHIBITOR-RESISTANT MELANOMAS). These authors (R.F.K., R.A.S., G.V.L., and A.R.) have received honoraria from or served as consultants to pharmaceutical firms (Roche-Genentech, GlaxoSmithKline).

Author contributions: H.S., W.H. X.K., A.H. G.M. designed and performed experiments and analyzed data. R.C.K., T.C., R.G., D.B.J, K.B.D, M.C.K., J.A.S., R.F.K., G.V.L., N.V.B., J.A.G., B.C., A.R., and R.S.L. recruited patient volunteers and/or provided reagents/tissues. All authors contributed to manuscript preparation. R.S.L. designed experiments and research aims, analyzed data, and wrote the paper.

melanomas. Distinct molecular lesions, in both core drug escape pathways, were commonly detected concurrently in the same tumor or among multiple tumors from the same patient. Beyond harboring extensively heterogeneous resistance mechanisms, melanoma re-growth emerging from BRAF inhibitor selection displayed branched evolution marked by altered mutational spectra/signatures and increased fitness. Thus, melanoma genomic heterogeneity contributes significantly to BRAF inhibitor treatment failure, implying upfront, co-targeting of two core pathways as an essential strategy for durable responses.

Keywords

BRAF; MAPK; PI3K-PTEN-AKT; clonal heterogeneity; melanoma; acquired BRAF inhibitor resistance

Introduction

Approximately 50% of metastatic melanomas harbor BRAF V600 mutations, most commonly a V600E substitution (1), which hyperactivate the mitogen-activated protein kinase (MAPK) pathway and result in oncogene addiction. BRAF inhibitors, such as vemurafenib and dabrafenib, can elicit highly reproducible objective anti-tumor responses in the majority of treated patients, but the durability of response is short (median 7 months) and limited by acquired drug resistance, resulting in disease progression (DP) (2-5).

Earlier studies have identified specific mechanisms of BRAF inhibitor resistance in melanoma (6-17), which may reflect two different biological processes: i) early intrinsic resistance or adaptive tumor response, and ii) late acquired resistance. An example of the adaptive response is the upregulation of receptor tyrosine kinases. Reported mechanisms of acquired BRAF inhibitor resistance in melanoma support the notion of MAPK pathway reactivation (18). Key mechanisms include emergence of mutant *BRAF*-concurrent *RAS (7)* or *MEK (*13*)* mutations and mutant *BRAF* amplification (11) or alternative splicing (8, 11), but the relative contribution of these mechanisms to clinical disease progression is unknown. Moreover, a clinical strategy to mitigate acquired BRAF inhibitor resistance by combined BRAF and MEK inhibition, although prolonging tumor suppression, is still beset by acquired drug resistance (19), suggesting MAPK-alternate escape route(s).

Cancer genomic heterogeneity in individual patients and tumors exists on a time-and-spatial continuum, an understanding of which has important consequences for personalized cancer medicine (20, 21). How melanoma genomic heterogeneity under BRAF inhibitor selective pressure contributes to acquired resistance is unknown. This clonal evolutionary process in response to targeting of a dominant oncogene addiction pathway has not been characterized at the landscape or single-nucleotide levels. Defining the major molecular lesions (both known and novel), their core pathways, and the extent of melanoma genomic diversification underlying acquired BRAF inhibitor resistance represent a key benchmark for the further clinical development of BRAF inhibitor-based therapeutic strategies.

Results

Melanomas reactivate MAPK or upregulate PI3K-AKT to acquire BRAF inhibitor resistance

We analyzed 100 tumor samples from 44 patients (median progression free survival or PFS = 145 days; range = 84 to 489) (Table 1; Fig. 1A; Supplementary Fig. S1 and Table S1) whose melanomas developed acquired resistance to either vemurafenib or dabrafenib monotherapy. These specimens consisted of 29 baseline (pre-treatment) and 71 progressive tumors (Table 1). We first performed detection of known mechanisms of acquired BRAF

inhibitor resistance, with the denominator of samples analyzed for each mechanism being slightly variable due to a small number of disease progressive tumors lacking patient-matched baseline tumors (for the detection of relative *BRAF* gene copies) or lacking RNA samples (for the detection of *BRAF* splicing) (Supplementary Table S2). We also generated 87 whole-exome sequence (WES) data sets (21 normal tissues, 22 baseline tumors, and 44 disease progressive tumors) only from patients who donated at least a triad of these tissues. Among these patients, 16 donated multiple geographically and/or temporally distinct disease progressive melanoma biopsies for this study, providing an opportunity to investigate tumor heterogeneity. We achieved a mean 107× coverage/base, 93.3% exome coverage at ≥ 15× (Supplementary Table S3) and a mutation-calling specificity of 96.2% as estimated by Sanger re-sequencing (Supplementary Table S4 and Fig. S2). Consistent with our earlier study (7), among 56 of 71 (79%) progressive tumors available for analysis by deep sequencing of all 18 *BRAF* exons, no (0 of 56 or 0%) *BRAF V600E/K*-secondary mutations were detected, but persistence of the same *BRAF V600E/K* mutations detected at baseline was noted in all 71 of 71 (100%) progressive tumors, i.e., BRAF inhibitor therapy did not select for minor, preexisting “contaminating” wild type *BRAF* clones (Supplementary Table S2).

Among MAPK-reactivating mechanisms associated with acquired BRAF inhibitor resistance (Supplementary Table S2), *NRAS* mutations (G12D/R, G13R, Q61K/R/L) were detected in 13 of 71 (18%) progressive tumors and *KRAS* mutations (G12C, G12R, Q61H) in 5 of 71 (7%) progressive tumors (Supplementary Fig. S3). Mutant *BRAF* amplification (2-15 fold or 4-75 copies) was detected in 11 of 57 (19%) progressive tumors with patient-matched baseline tumors, and mutant *BRAF* alternative splice variants were found when novel exon boundaries (between 1/9, 1/11, 3/9) were detected in 6 of 48 (13%) progressive tumors with available patient-matched baseline tumor RNA. Also, *MEK1* activating mutations (K57N (22), C121S) were detected in 2 of 71 (3%) progressive tumors, with the latter only detectable by WES but not Sanger sequencing due to a low mutant allelic frequency (Supplementary Table S2, Table S3 and Fig. S2). From the WES data set, we defined recurrent *CDKN2A* loss (3 of 44 or 7% of progressive tumors) as a MAPK-reactivating mechanism given that one of its gene products, p16/INK4A, negatively regulates the MAPK pathway effector complex consisting of cyclin D and CDK4, which was implicated in BRAF inhibitor resistance (23). The minimal common region of these deletions harbored *CDKN2A* but few other genes (Supplementary Fig. S4). Among all the disease progressive samples where MAPK-reactivating molecular alterations were detected, their relative distribution of detection frequencies is estimated in Figure 1B. More broadly among all the disease progressive samples, *RAS*, *MEK* and *CDKN2A* mutations as well as mutant *BRAF* amplification or alternative splicing were detected at a 70% frequency and thus composed a core pathway of acquired BRAF inhibitor resistance through MAPK reactivation (Fig. 1C; Supplementary Table S5).

WES data enabled nomination of the PI3K-PTEN-AKT melanoma pathway as second core resistance pathway (Supplementary Fig. S5 and Tables S2, S5 and Table S6). *AKT1/3* mutations (Q79K, E17K) (Fig. 1D) were discovered in 2 of 44 progressive tumors subjected to WES and 0 of 27 remaining progressive tumors by Sanger sequencing of exons 3 and 4 (containing these plekstrin homology domain (PHD) mutations). *AKT3* copy number increase was not detected in any progressive tumor (Supplementary Table S2). Mutations in additional PI3K-AKT positive-regulatory genes (*PIK3CA*, *PIK3CG*) and in negative-regulatory genes (*PIK3R2*, *PTEN*, *PHLPP1*) (Fig. 1D-F) were detected in 10 of 44 progressive tumors. Overall, PI3K-PTEN-AKT pathway mutations, all validated by Sanger sequencing, constituted a second core acquired resistance pathway (at a 22% frequency), which overlapped with the MAPK core pathway (Fig. 1C).

Distinct genetic lesions arise during disease progression to activate AKT

We studied in-depth the altered signaling effects of several genetic lesions in the PI3K-PTEN-AKT pathway by analyzing their predicted structural impacts (Fig. 2). AKT1 Q79K has been detected in breast and endometrial carcinoma (24), but its functional impact has not been characterized. Based on structure modeling (Fig. 2A), AKT1 Q79K in the PHD moved toward negatively charged phosphates of the Ins(1,3,4,5)P_4 by 4.02 Å when bound, suggesting enhanced lipid binding as K79 moved toward the 4- and 5-phosphates of PIP_3. In Apo AKT1 Q79K, the acidic E17 forms an ionic interaction with basic K14, “tightening” the closed conformation. With Ins(1,3,4,5)P_4 binding, R86 moved towards the 4-phosphate and K14 towards 3- and 4-phosphates (25). Superimposition of the apo and ligand-bound conformations showed that Q79K moved toward 4- and 5-phosphates in the latter. Notably, the PHD of PDK1, which contains a positively-charged arginine (R521) at its AKT1 Q79-homologous position, showed a higher affinity for PtdIns(3,4,5)P_3 than for PtdIns(3,4)P_2 (26), consistent with the prediction that AKT1 Q79K engages the 5-phosphates of PIP_3 during lipid binding. Indeed, a PHD domain harboring the Q79K substitution displayed enhanced recruitment to the cell surface compared to the wild type PHD (27). The somatic heterozygous AKT1 Q79K mutation (Supplementary Fig. S5) detected in melanoma during disease progression on BRAF inhibitor therapy is thus predicted to be a gain-of-function mutation.

PIK3CA D350G has been detected in breast, endometrial, pancreatic and colorectal carcinomas (24). Our structure modeling predicts that this somatic heterozygous mutant detected in disease progressive melanoma is also a gain-of-function mutation (Fig. 2B) in that the D350G substitution disrupting a critical interaction with a conserved serine (S565 in PIK3R2) in its negative regulator such as PIK3R1 (p85α) or PIK3R2 (p85β). On the other hand, we detected a somatic PIK3R2 heterozygous mutation (N561D) which is predicted to disrupt a hydrophobic interaction between PIK3R2 N561 with the PIK3CA N345 (Fig. 2C). PIK3R2 mutations, including N561D, are frequently detected in endometrial cancer (28). In addition to PTEN large-scale deletion and frame-shift (resulting in early termination), a PTEN M134 single amino acid delection was detected in a melanoma with acquired BRAF inhibitor resistance. This M134 deletion is predicted to disrupt the P loop which is critical for its phosphatase activity (Fig. 2D). Consistent with a critical role for PTEN, M134 subsitution mutation recurs in both endometrial and colorectal carcinomas (24).

We then directly analyzed these predicted functional mutants in the PI3K-PTEN-AKT pathway by introducing them into melanoma cell lines and detecting activated AKT (p-AKT Thr308) (Fig. 3A). Stable over-expression of AKT1 E17K or Q79K and AKT3 E17K in the M229 ^{V600E}*BRAF* human melanoma cell line increased p-AKT Thr308 levels, whereas wild type AKT1 or AKT3 over-expression did not or only minimally. In addition, stable over-expression of disease progression-specific PIK3CA mutants (D350G, E545G) and PIK3R2 mutant (N561D) increased the p-AKT level. Three types of *PTEN* genetic hits correlated with acquired BRAF inhibitor resistance: *PTEN* CN loss (Fig. 1F), frameshift mutation (fs 40), and single codon deletion (M134del) (Fig. 1D). The effects of these alterations were tested by stable knockdown of wild type *PTEN* expression in M229, which increased the p-AKT level. In contrast, stable over-expression of wild type PTEN, but not PTEN M134del, in the ^{V600E}*BRAF* human melanoma cell lines M249 and WM2664 suppressed the p-AKT levels. Melanoma cultures (VUB164 MEL A, B and C) derived from patient #43 tumor biopsies (baseline, disease-progressive tumors 1 and 2) displayed the same *PTEN* wild type (baseline) and M134del (DP1 and 2) genotypes (Supplementary Fig. S6). Consistently, VUB164 B and C, relative to VUB A, displayed elevated levels of p-AKT, which was reversed upon the stable overexpression of wild type PTEN. In available formalin-fixed

paraffin-embedded tissues, the detection of *AKT1* Q79K and *AKT3* E17K, *PTEN* CN loss or frame shift, and *PIK3R2* N561D was associated with elevated levels of p-AKT (Fig. 3B).

We also tested whether the detected functional molecular alterations would alter BRAF inhibitor sensitivity (Fig. 3C). Whereas AKT1 wild type over-expression had no effect on vemurafenib sensitivity, AKT1 Q79K or E17K and AKT3 E17K over-expression conferred vemurafenib resistance. *PTEN* knockdown in the *PTEN* wild type M229 cell line conferred vemurafenib resistance, and *PTEN* re-introduction into the *PTEN* non-expressing WM2664 cell line conferred vemurafenib sensitivity. Also, over-expression of PIK3CA D350G and E545G, as well as the positive control mutant PIK3CA E545K, conferred vemurafenib resistance when compared to the vector or PIK3CA wild type. Over-expression of wild type PIK3R2 expectedly suppressed the baseline p-AKT level, where as over-expression of PIK3R2 N561D not only did not suppress the baseline p-AKT level but also hyper-elevated it in WM2664 (Fig. 3A). Accordingly, when treated with vemurafenib, WM2664 over-expressing PIK3R2 N561D was more resistant to BRAF inhibition compared with WM2664 introduced with the vector or wild type PIK3R2 (Fig. 3C).

Tumor heterogeneity and branched evolution contribute to acquired BRAF inhibitor resistance

A molecular lesion in the MAPK and the PI3K-PTEN-AKT pathway could be detected in 70% and 22% of the progressive tumors, respectively, but tumor heterogeneity was notable, suggesting clonal heterogeneity and/or collaborative mechanisms (Fig. 1C). In 9 of 44 (20%) patients, at least two mechanisms of resistance were detected in the same patient (same or distinct progressive tumors) (Supplementary Table S2). This is an under-estimate of the true extent as only one progressive tumor was sampled in most patients and some progressive tumors were not amenable to all types of analysis. In 8 of these 9 patients, alterations in both core pathways were detected. In the subset of patients from whom multiple progressive samplings were feasible (n = 16 patients; Fig. 4A), 13 of 16 (81%) of patients harbored multiple mechanisms of resistance.

To investigate temporal and spatial tumor heterogeneity underlying acquired BRAF inhibitor resistance, we performed a whole exome-wide phylogenetic analysis of tissue biopsies from patient #37 (Fig. 4B and 4C) and other patients (Fig. 4D). Patient #37 had multiple cutaneous metastases and was started on the BRAF inhibitor dabrafenib in November 2010. On day 14, every single metastatic nodule had flattened, and the anti-tumor response was durable until day 383. Biopsies were performed on two baseline, two residual disease (RD1/2), and nine disease-progressive (DP) tumors. DP8 and 9 were the first subcutaneous (vs. cutaneous) metastases and presaged the onset of neurologic symptoms and brain metastasis in December 2012 (Fig. 4B).

Whole-exome, deep sequencing of gDNAs from blood, two baseline tumors and nine progressive tumors which spanned 726 days of BRAF inhibitor selection resulted in a mean coverage of 117.5× (StdDev = 38.7x; range = 44.1-175.5x). To infer clonal relationships among progressive and baseline tumors, we collated unambiguous somatic mutations which were private or unique in at least one progressive tumor. This resulted in a collection of 360 SNVs and 5 INDELs which engendered a parsimony-based phylogenetic tree (Fig. 4C). The root node (origin of radii) represented the last common ancestral (LCA) node harboring 2,393 SNVs and 12 indels (with respect to the normal sample) which were shared by all the baseline and progressive tumors. Without exception, all progressive tumors followed branched (vs. linear) evolution in this patient and others studied (Fig. 4D and Supplementary Fig. S7 and S8). The average distance of a baseline tumor from the LCA node (5.3 SNVs) of patient #37 was less than that of a progressive tumor from the LCA node (39.3 SNVs), suggesting clonal diversification associated with an increased mutational burden in certain

aberrant clones. Interestingly, the extent of genetic diversification of the progressive tumors was not co-linear with their timing of clinical emergence.

At least five drivers of acquired BRAF inhibitor resistance accounted for this patient's clinical relapse, including four characterized mechanisms and at least one additional but unknown mechanism (presumably shared by DP8/9). Thus, a single disease-progressive biopsy would have revealed only 1 of 5 (20%) drivers of acquired resistance. These ancestral relationships were further supported by several observations: i) three *KRAS* mutations were identical, supportive of DP2/5/6 diverging from a common, most recent ancestral node, ii) two mutant *BRAF* amplification events were similar in amplitude and amplicon size (Supplementary Fig. S9), supportive of DP1/3 evolving from a common, most recent ancestral node, and 3) two mutant *BRAF* alternative splicing events were associated with distinct novel exon-exon boundaries, supportive of convergent evolution for DP4/7 (Fig. 5A).

Disease progressive melanomas display variable ERK activation and increased proliferation

To examine how the genetic and mechanistic heterogeneity (Fig. 5A) correlated with tumor phenotypes, we assessed the relative levels of cell cycle progression marker Ki-67 (Fig. 5B) and the activated MAPK signaling marker p-ERK (Fig. 5C). Interestingly, when compared with the baseline tumor, the residual tumors (RD1 and RD2) displayed little to no Ki-67 staining, suggesting tumor proliferative dormancy. Invariably, the fraction of nuclei with Ki-67 staining was dramatically higher in the progressive tumors compared to that in the baseline tumor in patient #37 and the majority of other tumor pairs (Supplementary Fig. S10). This suggests that BRAF inhibitor-related genomic diversification, altered mutational load (e.g., DP9), mutagenic processes (e.g., DP3/6/9), and/or epigenetically alterations (e.g., DNA methylation-driven differential gene expression; unpublished data) may contribute to this observed increased in tumor fitness. Specifically, the extensive genetic divergence of DP3 (marked by LOHs; data not shown) and DP9 (marked by SNVs) correlated with the highest proliferative indices. The highest levels of nuclear p-ERK were observed in those progressive tumors where *KRAS* mutations were detected (Fig. 5A). Interestingly, DP8/9, with unknown drivers of BRAF inhibitor resistance, displayed minimal nuclear or cytoplasmic p-ERK staining.

The mutational spectra and signatures of disease progression-specific mutations are altered

Metastatic melanoma is marked by one of the highest mutational burdens seen across human malignancies, and ultraviolet (UV)-induced DNA damage, especially C > T transition mutations occurring within a dipyrimidine context, contributes to a dominant (> 90%) fraction of all nsSNVs (29). Hence, we investigated the mutational spectra before and after BRAF inhibitor therapy. We found that both baseline tumors from patient #37 (as well as all 22 baseline tumors with WES data) harbored a predominance of C > T transition mutations (Fig. 6A) with preference for a dipyrimidine motif (Fig. 6B). In contrast, the mutation spectra of disease progression-specific SNVs were significantly altered, with a relative reduction in C > T transitions and increase in other transition and transversion mutations (Fig. 6A). Moreover, C > T transitions found in the progressive tumors displayed an attenuated dipyrimidine motif (Fig. 6B and 6C), indicating disparate, non-UV related mutagenic processes.

Discussion

Our study supports MAPK reactivation as a major pathway of acquired BRAF inhibitor resistance in melanoma but also uncovers multiple genetic "hits" in the PI3K-PTEN-AKT pathway, nominating it as a second, *bona fide*, core pathway of late drug resistance. Tumor heterogeneity contributed substantially to acquired BRAF inhibitor resistance and occurred at the levels of geographically and temporally distinct escape sub-clones within the same patient and tumor. Among nine disease-progressive tumor biopsies in patient #37, 277 of 360 (77%) of high-confidence somatic SNVs used to reconstruct phylogeny were unique to only one disease-progressive melanoma.

Genomic diversification culminated in multiple molecular lesions driving drug resistance and likely malignancy. Multiple mechanisms of acquired resistance being detected in the same tumor biopsy implies collaborative roles or tumor sub-clonal heterogeneity. We expect more heterogeneous and functional genetic variants in the MAPK and PI3K-PTEN-AKT pathway components to be described as more patients and their biopsies are subjected to in-depth sequence and molecular analyses. Certain novel genetic variants, such as PHLPP1 K596E, may impact both core pathways. Although PHLPP is a phosphatase for AKT and S6K, it may also repress phosphorylation of ERK (30). Extensive branched evolution, implying a paucity of common driver mutations, challenges efforts to monitor solid cancer heterogeneity, which may be aided by recent advances in liquid biopsies of circulating tumor cells (31) or DNA (32) coupled with genomic analysis. Evidence of non-MEK-dependent survival and increasing clonal fitness in response to BRAF inhibitor therapy may help explain why i) the combination of BRAF and MEK inhibitors in BRAF inhibitor-progressors can only induce low rates of secondary responses with limited durability (33) and ii) upfront treatment with the combination of BRAF and MEK inhibitors in drug-naïve patients, albeit superior to either agent alone, is still beset eventually with acquired drug resistance (19).

In acquired BRAF inhibitor resistance, the proportion of melanomas harboring MAPK-reactivating molecular lesions was greater than that harboring PI3K-AKT-upregulating lesions. This relative distribution may stem from the early effects of therapy on these core pathways. Vemurafenib is known to suppress p-ERK in the majority of melanomas early during treatment (18, 34); hence, a majority of BRAF-inhibited melanomas would be under duress to reactivate p-ERK. In other work, we have shown that MAPK pathway inhibition can induce p-AKT levels within days of therapy and that gain-of-function AKT1 mutants most robustly conferred BRAF inhibitor resistance where this adaptive response was weak (27). Thus, the selective pressure for PI3K-AKT-upregulating genetic lesions may be tempered by tumor context-dependent AKT-dependent adaptive responses.

BRAF inhibitors are not known to be directly mutagenic to the melanoma genome but may engender secondary causes of DNA mutagenesis such as reactive oxygen species (ROS) production (35) or alterations in DNA methylation (36) and histone modifications (both of which could influence mutation sites and rates (37, 38). More likely, the alterations in the disease progression-specific mutational spectra and signatures reflect pre-existing minor (and lower fitness) sub-clones and/or the consequences of mutagenic processes (distinct from UV) more dominant throughout late-temporal malignant progression.

In conclusion, *BRAF* mutant melanomas acquire BRAF inhibitor resistance via upregulation of both MAPK and PI3K-AKT pathways and genomic diversification resulting in branched evolution and increased tumor fitness. These data strongly support upfront co-targeting of both drug escape pathways in *BRAF* mutant melanoma and imply a similar rationale to manage genetically complex human malignancies.

Methods

Analyses of tumor specimens

We evaluated 100 tumor biopsies from 44 patients. All 71 progressive tumors were examined for *BRAF* secondary mutations and known mechanisms of MAPK reactivation including *RAS/MEK* mutations by Sanger sequencing and mutant *BRAF* amplification by quantitative genomic DNA PCR or its alternative splicing by Sanger detection of novel exon-exon boundaries in the complementary DNAs (with exceptions noted in Supplementary Table S2). For analysis of known mechanisms such as *RAS* hotspot mutations, the denominator for analysis included all progressive tumor samples (inclusive of 24% of disease progressive tumors without patient-matched baseline tumor samples) since such mechanisms have been well-validated previously to be generally disease progression-specific in the acquired resistance setting. To nominate novel genetic alterations causing acquired resistance, baseline (n = 22) coupled with progressive (n = 44) tumors from 21 of 44 (48%) patients with available normal tissues were whole-exome sequenced (WES) (Table 1). Genetic variants analyzed functionally were validated by Sanger sequencing. P-AKT (Cell Signaling Technology #4060), p-ERK (Cell Signaling Technology #4376) and Ki-67 (Dako #M7240) levels were assessed by immunohistochemistry. All patients provided written informed consent.

Accounting of mechanisms and core pathways

For the MAPK-reactivating mechanisms (Fig. 1B), the detection frequencies of each mechanism (*NRAS* 18%, *KRAS* 6%, *BRAF* amp. 19%, *BRAF* alt. spl. 13%, *MEK1/2* 1%, CDKN2A 7%) were tallied, resulting in 64% (18+6+19+13+1+7=64). This normalized for the variable denominators or samples tested for each mechanism, as determined by the particular assay capability or tissue and whole exome sequence availabilities (Supplementary Table S2). The detection frequency of each mechanism (e.g., RAS 18% +6%=24%) was then divided by the total detection frequency (64%) to derive the pie chart shown in Figure 1B. Accounting of core pathway frequencies and their overlap incorporated samples with unknown mechanisms as shown in Figure 1C (Supplementary Tables S2 and S4). Disease progressive samples were designated as “unknowns” if all assays, including whole exome sequencing, were applied successfully. This determination avoided an over-estimation of the unknown frequency.

Whole-exome sequencing and variant-calling

For exome alignment, all samples were pair-end sequenced with length 2×100 bps except for samples from Patients #9 and #11 (2×76 bps reads) (Supplementary Table S3). The sequences were aligned to the hg19 UCSC reference genome using the NovoAlign software (NovoCraft Tech. version 2.08.01). The aligned BAM were filtered for PCR duplicates, INDEL-realigned, and score calibrated using the GATK tools (39), Samtools and Picard software following the protocol listed on the GATK website (39). Single nucleotide variants (SNVs) were called using a combination of the Unified Genotyper (UG) tool of GATK (with a Fisher’s Exact Test post-processing filter or GATK-UGF) (39), MuTect (40) and VarScan2 (41). INDELS (small insertion and deltions) were called using the combined calls of GATK-UGF, SomaticIndelDetector of GATK (IndelLocator) (40) and VarScan2. We leveraged the combined strength of these programs by nominating all mutations that were called by at least two of the three SNV/INDEL callers, resulting in high-confidence calls. LOH (loss of heterozygosity) calls on SNVs and INDELs were computed using GATK-UGF and VarScan2 (as MuTect and SomaticIndelDetector do not report them), resulting high-confidence LOH calls.

For GATK-UGF, we processed BAM files (normal of all patients, baseline, DP) and, using one-sided Fisher's Exact Test (P value cut-off ≤ 0.01), we retained only SNVs/INDELs whose mutant allele fraction at a SNV/INDEL position in the DP was significantly larger than that in the baseline and normal samples. Among these retained positions, DP-specific SNVs/INDELs were called when the genotype in the DP sample was heterozygous while the genotypes in the baseline and normal were the same and homozygous. Baseline-specific SNVs/INDELs were defined similarly between the baseline and normal samples. DP-LOH events were called on baseline-specific SNVs/INDELs whose mutant alleles (non-normal and non-reference) were significantly enriched in the DP (P value cut-off ≤ 0.01). LOH on germline SNV/INDEL positions in the normal sample were excluded from analysis. To avoid artefactual SNVs/INDELs from low coverage areas, we only report DP-specific and DP-LOH events with coverage ≥ 15 and SNV/INDEL score ≥ 30 (in phred scale) in the DP, baseline and normal samples.

We also ran VarScan2 on each DP BAM file with the baseline (1st run) and with normal (2nd run) as the reference BAM file. We allowed low-frequency variants (frequency ≥ 0.05) to pass as long as they met the default p-value cut-off. High-confidence calls were selected by the *processSomatic* and *fpfilter.pl* post-processing in accordance with VarScan2. We collected the DP-specific calls by intersecting the high-confidence SNV, INDEL, and LOH calls from both runs. For MuTect based SNV calling, we used the default parameters for both runs and collected the mutations that were annotated as "KEEP" in both runs as DP-specific SNVs. For GATK Somatic INDEL Detector-based INDEL calling, we likewise used the default parameters for both runs. Mutations that were annotated as "SOMATIC" in both runs were defined as DP-specific Baseline-specific INDELs were similarly collected by comparing the baseline vs. normal BAM files.

Shortlisted SNVs and INDELs were annotated by Oncotator[9]. Nucleotide and amino acid conservations were annotated by the phyloP (42) and polyphen2 (43) scores respectively. Mutations occurring in globular domain were listed based on domain boundaries in INTERPRO release 39.0. The nominated DP-specific and DP-LOH SNVs/INDELs were reviewed manually and visualized using IGV. SNVs/INDELs in regions with high conservation (polyphen2 ≥ 0.85 or PhyloP ≥ 1.8) were further studied by functional assays and structure-based homology modeling. A subset consisting of 108 non-silent, coding mutations was selected for Sanger re-sequencing to estimate the specificity of our SNV/INDEL-calling procedure.

Copy number analysis intersected calls made by ExomeDepth (44) and ExomeCNV (45). From ExomeCNV, we used a fold ratio cutoff of 1.75 for amplification and 0.625 for deletion (2-fold amplification and deletion with a 25% normal tissue contamination). The CNV call of ExomeDepth was performed using defaults options, including the removal of common CNVs. DP-specific CNVs were computed using the DP samples as target and both the baseline and normal as references. The CNV calls were visualized using Circos.

For pathway annotations, we extracted canonical MAPK and PI3K-AKT pathway components (Supplementary Table S2) from the KEGG pathway database. Our gene set of PI3K-PTEN-AKT pathway included the genes directly interacting with PI3K, PTEN and AKT in KEGG's PI3K-AKT signaling pathway (KEGG ID: hsa04151). RAF1 (CRAF) was excluded as it was already included as a MAPK signaling pathway's gene. Our gene set of (classical) MAPK pathway includes the genes directly interacting with the RAS, RAF, MEK and ERK genes in KEGG's MAPK signaling pathway (KEGG ID: hsa04151).

Homology-based structural analysis

Based on crystal structure of apo and PIP_4 bound wild type AKT1 (46), homology structures of apo and PIP_4 bound ^{Q79K}AKT1 were obtained by SWISS-MODEL (47) using apo (1UNP) and PIP_4 bound AKT1 (1UNQ) as templates. Structure alignment was calculated based on the amino acid residues from Lys14 to Arg86 (PIP_4 binding segment). Homology structure of a hetero-dimer between PIK3CA (p110α) and PIK3R1/2 (p85α/β) was obtained based on the template (PDB entry 3HIZ) (48), and the alignments were based on full-length proteins. The PTEN M134del structure was modeled by the I-TASSER online server (49) based on the full-length crystal structure bound to tartrate (PDB entry 1D5R) (50).

Phylogenetic tree construction

We chose high-quality, unambiguous, DP-specific SNVs and INDELs and selected SNV/INDEL sites (not necessarily falling in coding region) which satisfied the followings in all the samples: 1) coverage ≥ 15, 2) for each site, at least one of the samples must have a different genotype call from the rest of the samples, 3) sites with homozygous genotype must have at most three reads and at most 5% of any mutant allele (assumed to be caused by sequencing error), 4) sites with heterozygous genotype must have mutant allele fraction ≥ 10% and ≥ four mutant allele reads (following a similar cut-off in VarScan2). These stringent criteria were meant to filter out ambiguous GATK genotype calls to produce an accurate phylogenetic tree. We chose the mutant allele (i.e. non-reference, non-normal) of each site as its representative haplotype and used it to build the most parsimonious phylogenetic tree using the PHYLIP program's dnapars subroutine. Tree drawing was done using the drawtree program in PHYLIP. Shared mutations shown in the phylogenetic trees were computed based on the branching structure. We verified our tree construction method by confirming that the phylogenetic tree's branching structure inferred for Pt #37 stayed the same over different cut-offs of coverage depths, mutant allele fractions, and counts on both heterozygous and homozygous sites.

Mutation signature analysis

We categorized the DP-specific SNVs and baseline-specific SNVs based on types of nucleotide transitions and transversions. To compute the UVB signature, we collected the ±2 bases with respect to the C→T transition SNV sites using samtools' view command on the BAM alignment files and subsequently building a positional nucleotide frequency motif which was visualized using the seqLogo R package. The center nucleotide in the motif showed the wild type allele, which, in the C→T transition case, was the nucleotide C. The character height in the motif logo was drawn proportionally to the information content of the mutation site.

Analysis of PI3K-PTEN-AKT pathway mutants

Stable expression and knockdown by lentiviral transduction were performed in the *BRAF* mutant melanoma cell lines, M229, M249, WM2664 and VUB164MEL (A, B, and C). The M cell lines were established at UCLA with Institutional Review Board approval and routinely authenticated by mitochondrial DNA sequencing. WM2664 and VUB164MEL cell lines were obtained from the Wistar Institute and the Ludwig Institute for Cancer Research (Brussels Branch) via Material Transfer Agreements and were not further authenticated except for verification of the *BRAF* mutant status. Protein lysates were then analyzed by Western blotting (antibodies for p-AKT Thr308, p-AKT Ser473, total AKT, p-ERK1/2 Thr202/Tyr204, total ERK, total PTEN were purchased from Cell Signaling Technology #4056, 4060, 4685, 9101, 9102, 9188, respectively; for FLAG, and TUBULIN from Sigma F1804 and T9026). Effect of vemurafenib (vs. dimethylsulfoxide) on cell survival was measured by MTT (3 days of drug exposure) or clonogenic assays (10 days). The p-values

of compared survival curves were calculated by Graphpad prism 4.0. The dose values were log-transformed and normalized. Non-linear regressions were performed with the sigmoidal dose-response model. $LogEC_{50}$ of each fitted curve was compared to that of vector control, and a p-value < 0.05 (F-test) was considered statistically significant.

Supplementary Material

Refer to Web version on PubMed Central for supplementary material.

Acknowledgments

We thank the patients for their participation and G. Bollag and P. Lin (Plexxikon Inc.) for providing PLX4032, Gulietta Pupo (MIA) & Donald Hicks (Vanderbilt) for technical assistance, Pam Lyle (Vanderbilt), Richard Scolyer (MIA) & Sharona Yashar (UCLA) for pathology expertise, and A. Villanueva (UCLA) for clinical data management.

Financial support: R. S. Lo is supported by a Stand Up To Cancer Innovative Research Grant, a Program of the Entertainment Industry Foundation (SU2C-AACR-IRG0409). Additional funding for R.S.L came the National Cancer Institute (K22CA151638, 1R01CA176111), Burroughs Wellcome Fund, American Skin Association, Melanoma Research Alliance, Sidney Kimmel Foundation for Cancer Research, Eli & Edythe Broad Center of Regenerative Medicine & Stem Cell Research, Ian Copeland Melanoma Fund, the Harry J. Lloyd Charitable Trust, and the National Center for Advancing Translational Sciences UCLA CTSI Grant UL1TR000124. Funding for R.S.L and A.R. came from National Cancer Institute (1P01CA168585), The Seaver Institute, the Wesley Coyle Memorial Fund, Louis Belley and Richard Schnarr Fund. Funding for A.R. came from the Dr. Robert Vigen Memorial Fund, the Garcia-Corsini Family Fund, and the Ruby Family Foundation. Funding for A.H. came from Association of American Cancer Institutes and American Skin Association. Funding for R.F.K. and G.V.L. came from National Health and Medical Research Council of Australia and Translational Research Program of the Cancer Institute New South Wales. Funding for J.A.S. came from the American Cancer Society Melanoma Research Professorship and NCI 5K24 CA097588 Midcareer patient oriented research award. Patient informed consent was obtained for the research performed in this study.

Abbreviation list

RD	residual disease
DP	disease progression
WES	whole-exome sequence
UV	ultraviolet

References

1. Davies H, Bignell GR, Cox C, Stephens P, Edkins S, Clegg S, et al. Mutations of the BRAF gene in human cancer. Nature. Jun 27; 2002 417(6892):949–54. [PubMed: 12068308]
2. Chapman PB, Hauschild A, Robert C, Haanen JB, Ascierto P, Larkin J, et al. Improved survival with vemurafenib in melanoma with BRAF V600E mutation. N Engl J Med. Jun 30; 2011 364(26): 2507–16. [PubMed: 21639808]
3. Flaherty KT, Puzanov I, Kim KB, Ribas A, McArthur GA, Sosman JA, et al. Inhibition of mutated, activated BRAF in metastatic melanoma. N Engl J Med. Aug 26; 2010 363(9):809–19. [PubMed: 20818844]
4. Hauschild A, Grob JJ, Demidov LV, Jouary T, Gutzmer R, Millward M, et al. Dabrafenib in BRAF-mutated metastatic melanoma: a multicentre, open-label, phase 3 randomised controlled trial. Lancet. Jul 28; 2012 380(9839):358–65. [PubMed: 22735384]
5. Sosman JA, Kim KB, Schuchter L, Gonzalez R, Pavlick AC, Weber JS, et al. Survival in BRAF V600-mutant advanced melanoma treated with vemurafenib. N Engl J Med. Feb 23; 2012 366(8): 707–14. [PubMed: 22356324]

6. Johannessen CM, Boehm JS, Kim SY, Thomas SR, Wardwell L, Johnson LA, et al. COT drives resistance to RAF inhibition through MAP kinase pathway reactivation. Nature. Dec 16; 2010 468(7326):968–72. [PubMed: 21107320]
7. Nazarian R, Shi H, Wang Q, Kong X, Koya RC, Lee H, et al. Melanomas acquire resistance to B-RAF(V600E) inhibition by RTK or N-RAS upregulation. Nature. Dec 16; 2010 468(7326):973–7. [PubMed: 21107323]
8. Poulikakos PI, Persaud Y, Janakiraman M, Kong X, Ng C, Moriceau G, et al. RAF inhibitor resistance is mediated by dimerization of aberrantly spliced BRAF(V600E). Nature. Dec 15; 2011 480(7377):387–90. [PubMed: 22113612]
9. Shi H, Kong X, Ribas A, Lo RS. Combinatorial treatments that overcome PDGFRβ-driven resistance of melanoma cells to B-RAF(V600E) inhibition. Cancer Research. 2011; 71(15):5067–74. [PubMed: 21803746]
10. Shi H, Moriceau G, Kong X, Koya RC, Nazarian R, Pupo GM, et al. Preexisting MEK1 exon 3 mutations in V600E/KBRAF melanomas do not confer resistance to BRAF inhibitors. Cancer Discov. May; 2012 2(5):414–24. [PubMed: 22588879]
11. Shi H, Moriceau G, Kong X, Lee MK, Lee H, Koya RC, et al. Melanoma whole-exome sequencing identifies (V600E)B-RAF amplification-mediated acquired B-RAF inhibitor resistance. Nat Commun. 2012; 3:724. [PubMed: 22395615]
12. Villanueva J, Vultur A, Lee JT, Somasundaram R, Fukunaga-Kalabis M, Cipolla AK, et al. Acquired Resistance to BRAF Inhibitors Mediated by a RAF Kinase Switch in Melanoma Can Be Overcome by Cotargeting MEK and IGF-1R/PI3K. Cancer Cell. Dec 14; 2010 18(6):683–95. [PubMed: 21156289]
13. Wagle N, Emery C, Berger MF, Davis MJ, Sawyer A, Pochanard P, et al. Dissecting therapeutic resistance to RAF inhibition in melanoma by tumor genomic profiling. J Clin Oncol. Aug 1; 2011 29(22):3085–96. [PubMed: 21383288]
14. Straussman R, Morikawa T, Shee K, Barzily-Rokni M, Qian ZR, Du J, et al. Tumour micro-environment elicits innate resistance to RAF inhibitors through HGF secretion. Nature. Jul 26; 2012 487(7408):500–4. [PubMed: 22763439]
15. Wilson TR, Fridlyand J, Yan Y, Penuel E, Burton L, Chan E, et al. Widespread potential for growth-factor-driven resistance to anticancer kinase inhibitors. Nature. Jul 26; 2012 487(7408): 505–9. [PubMed: 22763448]
16. Girotti MR, Pedersen M, Sanchez-Laorden B, Viros A, Turajlic S, Niculescu-Duvaz D, et al. Inhibiting EGF receptor or SRC family kinase signaling overcomes BRAF inhibitor resistance in melanoma. Cancer Discov. Dec 14.2013
17. Paraiso KH, Xiang Y, Rebecca VW, Abel EV, Chen YA, Munko AC, et al. PTEN loss confers BRAF inhibitor resistance to melanoma cells through the suppression of BIM expression. Cancer Res. Apr 1; 2011 71(7):2750–60. [PubMed: 21317224]
18. Trunzer K, Pavlick AC, Schuchter L, Gonzalez R, McArthur GA, Hutson TE, et al. Pharmacodynamic Effects and Mechanisms of Resistance to Vemurafenib in Patients With Metastatic Melanoma. J Clin Oncol. Apr 8.2013
19. Flaherty KT, Infante JR, Daud A, Gonzalez R, Kefford RF, Sosman J, et al. Combined BRAF and MEK Inhibition in Melanoma with BRAF V600 Mutations. N Engl J Med. Sep 29.2012
20. Aparicio S, Caldas C. The implications of clonal genome evolution for cancer medicine. N Engl J Med. Feb 28; 2013 368(9):842–51. [PubMed: 23445095]
21. Gerlinger M, Rowan AJ, Horswell S, Larkin J, Endesfelder D, Gronroos E, et al. Intratumor heterogeneity and branched evolution revealed by multiregion sequencing. N Engl J Med. Mar 8; 2012 366(10):883–92. [PubMed: 22397650]
22. Marks JL, Gong Y, Chitale D, Golas B, McLellan MD, Kasai Y, et al. Novel MEK1 mutation identified by mutational analysis of epidermal growth factor receptor signaling pathway genes in lung adenocarcinoma. Cancer Res. Jul 15; 2008 68(14):5524–8. [PubMed: 18632602]
23. Smalley KS, Lioni M, Dalla Palma M, Xiao M, Desai B, Egyhazi S, et al. Increased cyclin D1 expression can mediate BRAF inhibitor resistance in BRAF V600E-mutated melanomas. Mol Cancer Ther. Sep; 2008 7(9):2876–83. [PubMed: 18790768]

24. Forbes SA, Bindal N, Bamford S, Cole C, Kok CY, Beare D, et al. COSMIC: mining complete cancer genomes in the Catalogue of Somatic Mutations in Cancer. Nucleic Acids Res. Jan.2011 39:D945–50. Database issue. [PubMed: 20952405]
25. Thomas CC, Dowler S, Deak M, Alessi DR, van Aalten DM. Crystal structure of the phosphatidylinositol 3,4-bisphosphate-binding pleckstrin homology (PH) domain of tandem PH-domain-containing protein 1 (TAPP1): molecular basis of lipid specificity. Biochem J. Sep 1; 2001 358(Pt 2):287–94. [PubMed: 11513726]
26. Stephens L, Anderson K, Stokoe D, Erdjument-Bromage H, Painter GF, Holmes AB, et al. Protein kinase B kinases that mediate phosphatidylinositol 3,4,5-trisphosphate-dependent activation of protein kinase B. Science. Jan 30; 1998 279(5351):710–4. [PubMed: 9445477]
27. Shi H, Hong A, Kong X, Koya RC, Song C, Moriceau G, et al. A novel AKT1 mutation amplifies an adaptive melanoma response to BRAF inhibition. Cancer Discov. 2013 Submitted.
28. Cheung LW, Hennessy BT, Li J, Yu S, Myers AP, Djordjevic B, et al. High frequency of PIK3R1 and PIK3R2 mutations in endometrial cancer elucidates a novel mechanism for regulation of PTEN protein stability. Cancer Discov. Jul; 2011 1(2):170–85. [PubMed: 21984976]
29. Hodis E, Watson IR, Kryukov GV, Arold ST, Imielinski M, Theurillat JP, et al. A landscape of driver mutations in melanoma. Cell. Jul 20; 2012 150(2):251–63. [PubMed: 22817889]
30. O'Neill AK, Niederst MJ, Newton AC. Suppression of survival signalling pathways by the phosphatase PHLPP. FEBS J. Jan; 2013 280(2):572–83. [PubMed: 22340730]
31. Hou S, Zhao L, Shen Q, Yu J, Ng C, Kong X, et al. Polymer nanofiber-embedded microchips for detection, isolation, and molecular analysis of single circulating melanoma cells. Angew Chem Int Ed Engl. Mar 18; 2013 52(12):3379–83. [PubMed: 23436302]
32. Murtaza M, Dawson SJ, Tsui DW, Gale D, Forshew T, Piskorz AM, et al. Non-invasive analysis of acquired resistance to cancer therapy by sequencing of plasma DNA. Nature. May 2; 2013 497(7447):108–12. [PubMed: 23563269]
33. Lo RS, Ribas A, Long GV, Ballotti R, Berger M, Hugo W, et al. Meeting report from the Society for Melanoma Research 2012 Congress, Hollywood, California. Pigment Cell Melanoma Res. Apr 4.2013
34. Bollag G, Hirth P, Tsai J, Zhang J, Ibrahim PN, Cho H, et al. Clinical efficacy of a RAF inhibitor needs broad target blockade in BRAF-mutant melanoma. Nature. Sep 30; 2010 467(7315):596–9. [PubMed: 20823850]
35. DeNicola GM, Karreth FA, Humpton TJ, Gopinathan A, Wei C, Frese K, et al. Oncogene-induced Nrf2 transcription promotes ROS detoxification and tumorigenesis. Nature. Jul 7; 2011 475(7354): 106–9. [PubMed: 21734707]
36. Hou P, Liu D, Dong J, Xing M. The BRAF(V600E) causes widespread alterations in gene methylation in the genome of melanoma cells. Cell Cycle. Jan 15; 2012 11(2):286–95. [PubMed: 22189819]
37. Schuster-Bockler B, Lehner B. Chromatin organization is a major influence on regional mutation rates in human cancer cells. Nature. Aug 23; 2012 488(7412):504–7. [PubMed: 22820252]
38. Walsh CP, Xu GL. Cytosine methylation and DNA repair. Curr Top Microbiol Immunol. 2006; 301:283–315. [PubMed: 16570853]
39. McKenna A, Hanna M, Banks E, Sivachenko A, Cibulskis K, Kernytsky A, et al. The Genome Analysis Toolkit: a MapReduce framework for analyzing next-generation DNA sequencing data. Genome Res. Sep; 2010 20(9):1297–303. [PubMed: 20644199]
40. Cibulskis K, Lawrence MS, Carter SL, Sivachenko A, Jaffe D, Sougnez C, et al. Sensitive detection of somatic point mutations in impure and heterogeneous cancer samples. Nat Biotechnol. Mar; 2013 31(3):213–9. [PubMed: 23396013]
41. Koboldt DC, Zhang Q, Larson DE, Shen D, McLellan MD, Lin L, et al. VarScan 2: somatic mutation and copy number alteration discovery in cancer by exome sequencing. Genome Res. Mar; 2012 22(3):568–76. [PubMed: 22300766]
42. Pollard KS, Hubisz MJ, Rosenbloom KR, Siepel A. Detection of nonneutral substitution rates on mammalian phylogenies. Genome Res. Jan; 2010 20(1):110–21. [PubMed: 19858363]

43. Adzhubei IA, Schmidt S, Peshkin L, Ramensky VE, Gerasimova A, Bork P, et al. A method and server for predicting damaging missense mutations. Nat Methods. Apr; 2010 7(4):248–9. [PubMed: 20354512]
44. Plagnol, V. Available from: http://www.inside-r.org/packages/cran/ExomeDepth/docs/CallCNVs
45. Sathirapongsasuti JF, Lee H, Horst BA, Brunner G, Cochran AJ, Binder S, et al. Exome Sequencing-Based Copy-Number Variation and Loss of Heterozygosity Detection: ExomeCNV. Bioinformatics. Aug 9; 2011 27(19):2648–54. [PubMed: 21828086]
46. Milburn CC, Deak M, Kelly SM, Price NC, Alessi DR, Van Aalten DM. Binding of phosphatidylinositol 3,4,5-trisphosphate to the pleckstrin homology domain of protein kinase B induces a conformational change. Biochem J. Nov 1; 2003 375(Pt 3):531–8. [PubMed: 12964941]
47. Arnold K, Bordoli L, Kopp J, Schwede T. The SWISS-MODEL workspace: a web-based environment for protein structure homology modelling. Bioinformatics. Jan 15; 2006 22(2):195–201. [PubMed: 16301204]
48. Mandelker D, Gabelli SB, Schmidt-Kittler O, Zhu J, Cheong I, Huang CH, et al. A frequent kinase domain mutation that changes the interaction between PI3Kalpha and the membrane. Proc Natl Acad Sci U S A. Oct 6; 2009 106(40):16996–7001. [PubMed: 19805105]
49. Zhang Y. I-TASSER server for protein 3D structure prediction. BMC Bioinformatics. 2008; 9:40. [PubMed: 18215316]
50. Lee JO, Yang H, Georgescu MM, Di Cristofano A, Maehama T, Shi Y, et al. Crystal structure of the PTEN tumor suppressor: implications for its phosphoinositide phosphatase activity and membrane association. Cell. Oct 29; 1999 99(3):323–34. [PubMed: 10555148]

Significance

This study provides critical insights into how human *BRAF* mutant melanoma, a malignancy with marked mutational burden, escapes from BRAF inhibitors. Understanding the core resistance pathways and tumor heterogeneity, fitness and mutational patterns which emerge under drug selection lays a foundation to rationalize clinical studies and investigate mechanisms of disease progression.

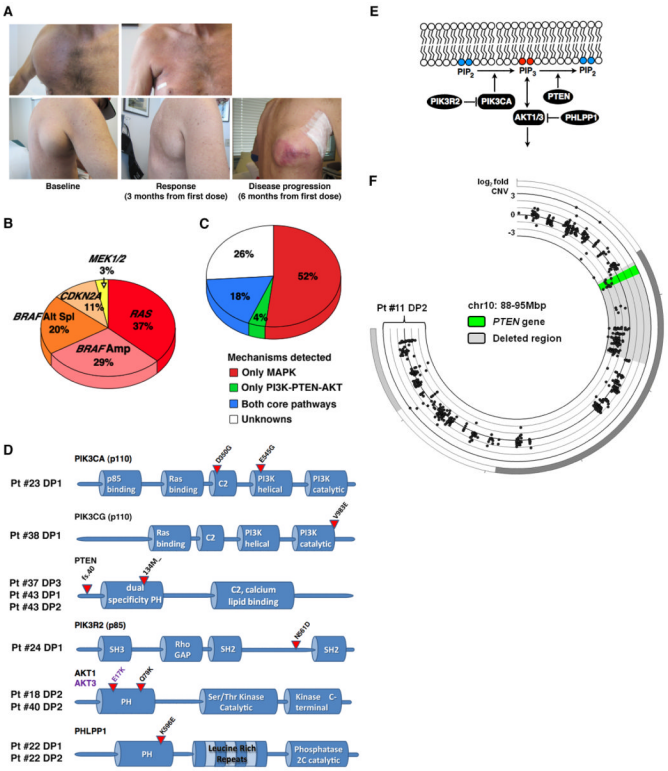

Figure 1.

Core melanoma escape pathways during disease progression on BRAF Inhibitor therapy. **A,** Representative photographs (patient #25) of initial vemurafenib response, incomplete response or residual and later acquired BRAFi resistance, which occurred at a site of incompletely shrunken tumor. **B,** The relative distribution of MAPK-reactivating mechanisms among disease progressive melanomas where such mechanisms were detected. **C,** The relative distribution of core pathways (MAPK vs. PI3K-PTEN-AKT) and hitherto unknown mechanisms among all melanomas featuring disease progression. **D,** Non-synonymous mutations in the PI3K-PTEN-AKT core drug escape pathway detected only in disease progression (DP) tumors. The schematics show the locations of mutations in the protein domain structures and their corresponding source patients and tissues. **E,** Signaling schematics of PI3K-PTEN-AKT pathway components mutated in biopsies of growing melanomas with acquired BRAF inhibitor resistance (PIK3CA, p110; PIK3R2, p85). **F,** Focal copy number loss of *PTEN* in DP melanoma of patient #11.

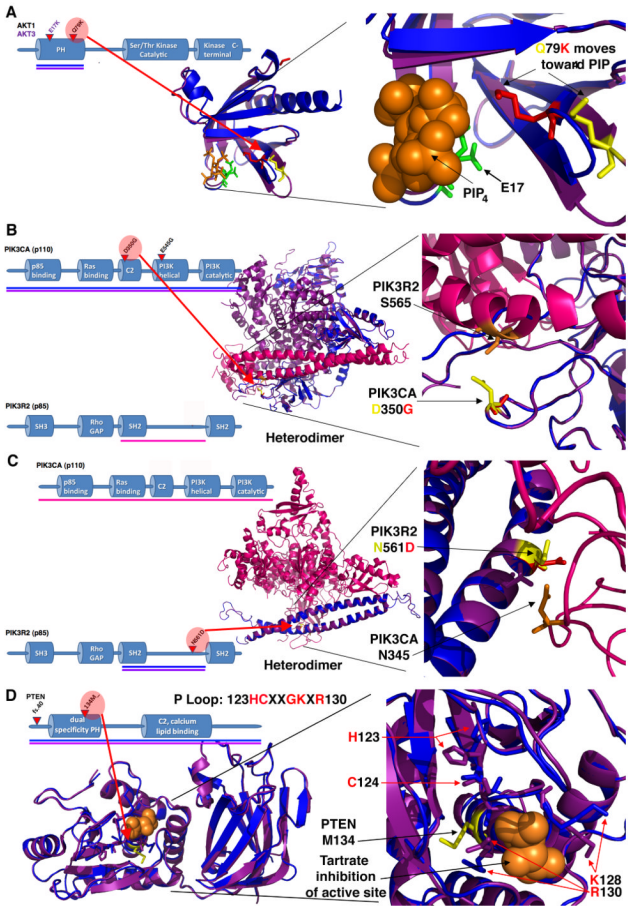

Figure 2. Structure-function models of novel mutants in the PI3K-AKT pathway

A, Schematic protein domains of AKT showing locations of E17K (AKT3) and Q79K (AKT1) substitutions in the PHD (underlined portion represented in 3D). Merged structures of Apo ^{Q79K}AKT1 (purple) and IP_4-bound ^{Q79K}AKT1 (blue) with zoomed-in image (PIP_4, orange) showing locations of E17 (green) and relative positions of WT Q79 (yellow) and mutant K79 (red). **B,** Schematic protein domains of PIK3CA (p110α) and PIK3R2 (p85) showing locations of the PIK3CA D350G (C2 domain) and E545G (helical domain) substitutions. Underlined portions of PIK3CA and homologous PIK3R1 represented as a 3D hetero-dimer (PIK3CA WT, purple; PIK3CA D350G, blue; niSH2 domain of PIK3R1 (p85α), magenta). A zoomed-in view of the interface between the C2 domain of PIK3CA and niSH2 domain of PIK3R2 suggesting the D350G (D350 yellow; G350 red) substitution likely abolishes a critical interaction with the highly conserved S565 (orange) of PIK3R2. **C,** Schematic protein domains of PIK3CA (p110α) and PIK3R2 (p85) showing location of the PIK3R2 N561D substitution in the iSH helical linker domain. PIK3CA WT (aa 31-515; magenta) in complex with a merged niSH2 domain structure of PIK3R2 WT (purple) and PIK3R2 N561D (blue). A zoomed-in view of the interface between the C2 domain of PIK3CA and niSH2 domain of PIK3R2 showing the interaction between PIK3R2 N561 (yellow) and PIK3CA N345 (orange) being disrupted by the PIK3R2 N561D mutant (red). **D,** Schematic protein domains of PTEN showing the locations of the frameshift mutation in codon 40 and the deletion of M134. Merged structures of the full-length PTEN WT (purple) with M134 highlighted (yellow) and PTEN M134del (blue) in the dual-specificity phosphatase domain bound by the inhibitor tartrate (orange). A zoomed-in view showing how deletion of the highly conserved M134 (yellow) may destabilize an alpha helical

structure proximal to the P loop and alters the critical side chain conformations of the P loop, which is critical for phosphatase activity.

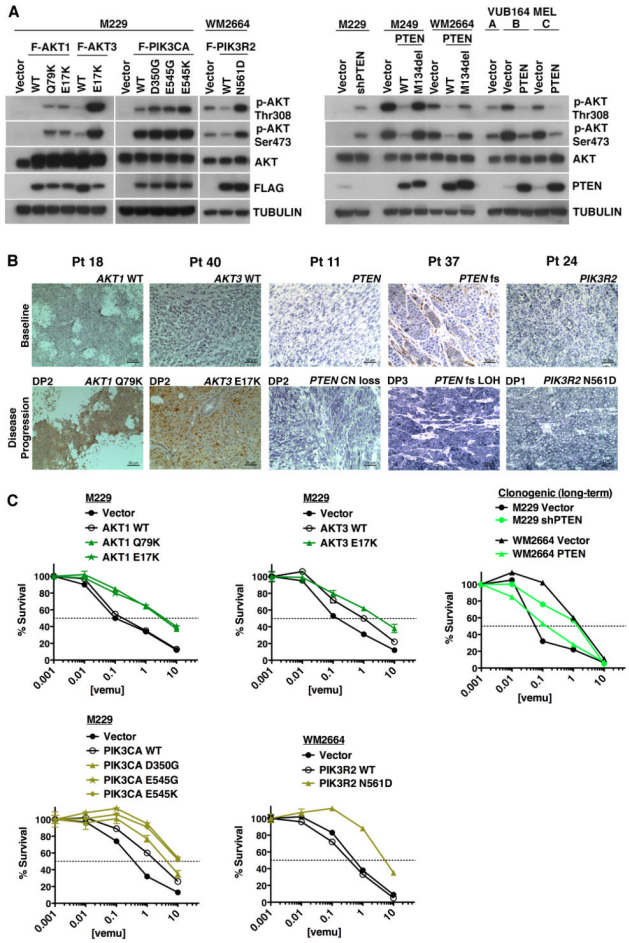

Figure 3.

Genetic alterations in the PI3K-PTEN-AKT pathway detected during disease progression and their functional impacts. **A,** Immunoblotting of protein lysates from ^{V600E}*BRAF* human melanoma cell lines (M229, WM2664, M249 and VUB MEL A, B, and C) stably expressing the indicated wild type or mutant genes and their impacts on phospho-AKT (also shown are total levels and TUBULIN serving as loading controls). **B,** Phospho-AKT (Ser473; brown, left two panels; grey/black, right threepanels) staining by immunohistochemistry (bar, 50 μM) in melanoma tissues harboring indicated genetic alterations in the PI3K-PTEN-AKT pathway during disease progression (relative to staining in melanomas before BRAF inhibitor therapy). **C,** The effects of stable over-expression of indicated AKT1/3, PIK3CA, PIK3R2 and PTEN constructs or stable PTEN knockdown (vs. empty vectors) on cellular sensitivity to vemurafenib-mediated growth suppression (error bars, SEM; P values of logEC_{50} of each construct vs. vector: AKT1 WT 0.2984, E17K 0.0006, Q79K 0.0001; AKT3 WT 0.0064, E17K 0.0033; PIK3CA WT < 0.0001, D350G 0.0148, E545G < 0.0001, E545K < 0.0001; PIK3R2 WT 0.8262, N561D < 0.0001).

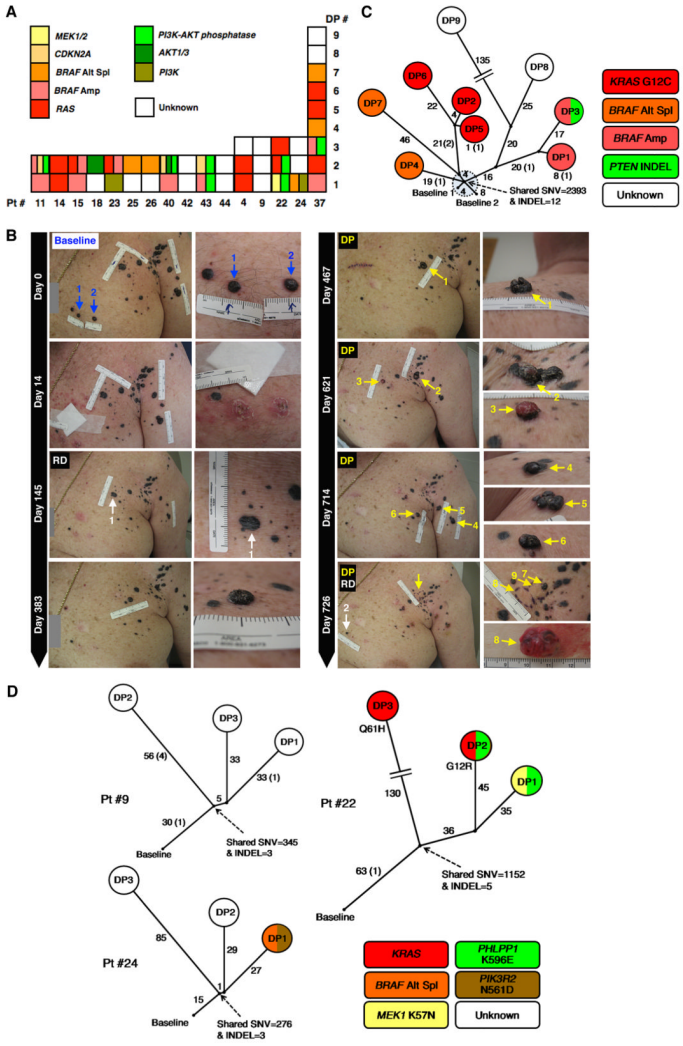

Figure 4.

Melanoma heterogeneity and branched evolution during the acquisition of BRAF inhibitor resistance. **A,** Detection of molecular mechanisms of acquired BRAF inhibitor resistance, grouped into core escape pathways, among temporally and geographically distinct disease progression (DP) melanoma biopsies from 16 patients. Intra-tumoral sub-clone heterogeneity vs. concurrence of molecular alterations cannot be distinguished in this analysis. **B,** Time course of metastatic melanomas to the skin in patient #37 responding to the BRAF inhibitor dabrafenib and the timing and sites of thirteen tumor biopsies (two baseline, two residual disease (RD) melanomas, and nine DP melanomas). Zoomed-in photographs highlight protuberant growths of specific metastatic foci, which together show temporal accretion of disease progression events. **C,** The phylogenetic relationships of the distinct baseline and DP melanomas in patient #37. Branch lengths are proportional to the number of somatic single nucleotide variants or SNVs (and INDELs in parenthesis) separating the branching points, and the sum of these SNVs and INDELs represent the collection of somatic variants unique or private in at least one tumor. The individual DP melanomas are color-coded by detection of distinct driver mechanisms of acquired BRAF inhibitor resistance. **D,** Whole-exome phylogenetic trees of tumor biopsies from additional patients (in addition to Pt #37) who donated multiple DP samples. In all three patients, DP tumors from the same patient displayed genomic diversification in a branching pattern. Pt

#22 DP2 harbored a KRAS G12R mutation while DP3 harbored a KRAS Q61H mutation, consistent with the tree showing the two DP tumors diverging early and independently acquiring distinct KRAS mutations (i.e., convergent evolution). Pt #22 DP1, which arose from the same sub-branch as DP2, acquired an activating MEK1 mutation (K57N) instead of a KRAS mutation. Pt #24 DP1 harbored a loss-of-function mutation in PIK3R2 as well as mutant BRAF alternative splicing, while the mechanism(s) of acquired resistance in DP2/3 remains unknown. Consistently, the tree branching pattern/distances indicate that DP1-3 shared few common mutations.

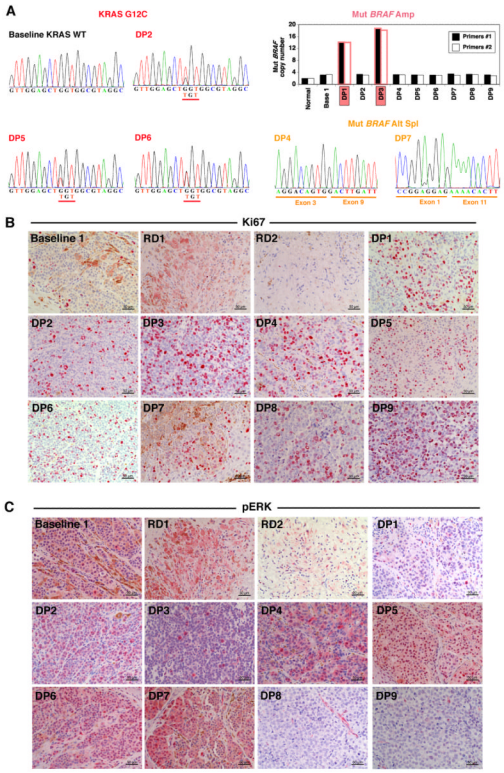

Figure 5.

Correlation between genotypes and phenotypes in melanoma biopsies from Patient #37. **A,** The detection of specific driver alterations in distinct disease progression (DP) melanomas and their relationships to the levels of Ki-67 (**B**) and p-ERK (**C**) detected by immunohistochemical staining (bar, 50 μM). Baseline 2 tumor, FFPE not available.

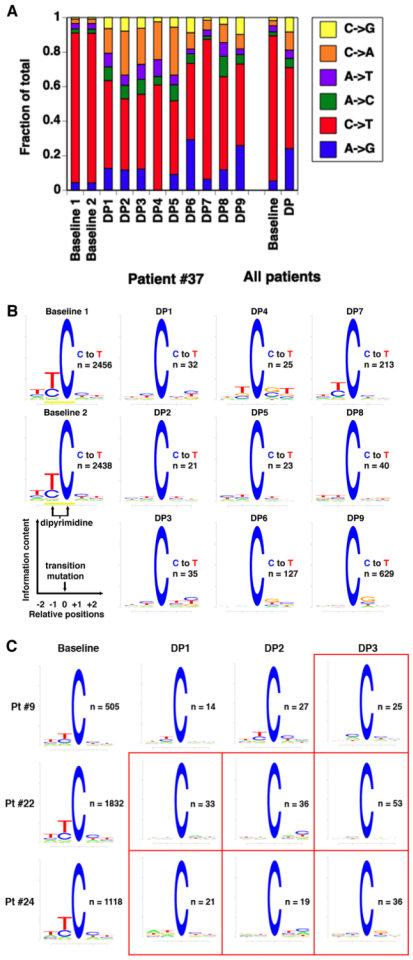

Figure 6.

The mutational spectra and signatures before versus after BRAF inhibitor therapy. **A,** The altered mutational spectra of baseline vs. DP melanomas in patient #37 as well as in all baseline vs. all DP melanomas with whole-exome sequence data (baseline tumors n = 22; DP tumors n = 44; Student t-test on the distributions of median fractions of A > G, C > T, A > C, A >T, C > A, C > G between baseline and DP were respectively 3.22×10^{-8}, 1.38×10^{-13}, 6.91×10^{-5}, 4.09×10^{-3}, 1.32×10^{-10}, and 1.50×10^{-5}). **B,** Detection of a dipyrimidine motif of C > T transitions (UV signature) in the baseline but not the DP melanomas of patient #37. Instead, certain DP melanomas displayed C > T transitions occurring in the CG dinucleotide motif. Motif analyses were centered on the C > T transitions and inclusive of −2 and +2 nucleotides. **C,** Detection of a dipyrimidine motif of C > T transitions (UV signature) in the baseline tumors but not in the majority of patient-matched DP tumors in three additional patients with multiple biopsies during disease progression. Instead, certain DP melanomas displayed C > T transitions occurring in the CG dinucleotide motif. Together with the observations made in Pt #37 (**B**), the loss of baseline-somatic dipyrimidine C>T UV signature mutations (among the DP-specific mutations, highlighted in red boxes in **C**) was estimated to occur at a frequency of 56%.

Table 1
Summary of clinical, tissue and study characteristics

	Total # (% of total)	Subset characteristics			
Patients	**44**		**Male**	**Female**	**Both**
		Patient Counts	31	13	44
		Median age (range)	59 (29-84)	53 (38-70)	59 (29-84)
		Median PFS (days)	149	183	145
		Median BOR	−47%	−63%	−53%
		Disease Stage			
		IIIc	1	1	2
		M1a	6	4	10
		M1b	1	2	3
		M1c	23	6	29
Tumor biopsies	100	Baseline biopsies		29 (28%)	
		Disease Progression (DP) biopsies		71 (72%)	
		DP biopsies with patient-matched baseline biopsies		55 (77%)	
Patients with multiple DP biopsies	16 (36%)	DPs / patient = 2		11 (69%)	
		DPs / patient = 3		4 (25%)	
		DPs / patient > 3		1 (6%)	
Patients with WES data from normal, baseline & DP tissues	21 (48%)	Normal tissues		21 (24%)	
		Baseline tumors		22 (25%)	
		DP tumors		44 (51%)	
		Total samples with WES		87	